Ocean Dynamics (2016) 66:795–810
DOI 10.1007/s10236-016-0951-1

Features and variability of the South China Sea western boundary current from 1992 to 2011

Qi Quan[1,2] · Huijie Xue[1,3] · Huiling Qin[1] · Xuezhi Zeng[4] · Shiqiu Peng[1]

Received: 29 September 2015 / Accepted: 21 March 2016 / Published online: 7 April 2016

Abstract Different from the traditional definition of the South China Sea western boundary current (SCSWBC), in this paper, only the southwestward and southward currents along the northern and western slopes in the SCS, which are closely associated with the basin-wide wind stress curl, are defined as the SCSWBC, while the flows on the southwestern shelf driven directly by the local wind stress are regarded as part of the shelf circulation. Using a new reanalysis dataset of the SCS in conjunction with the in situ and remote sensing data, the main features and variability of the SCSWBC from 1992 to 2011 were studied. Dictated by the prevailing monsoonal winds and in- and outflows, the SCSWBC in winter extended the full length of the western slope and reached its maximum intensity off the southeast coast of Vietnam, while in summer the main body of the SCSWBC was limited to the northern half of the western slope and merged with the northward coastal current to form the Vietnam Offshore Current (VOC) at about 12° N. Moreover, the respective seasonal patterns of the SCSWBC showed pronounced interannual variations in its structure, including the axis, the width, and the maximum depth. The strength of the SCSWBC, with the transport of -11.8 ± 3.5 Sv in winter and -3.0 ± 1.6 Sv in summer off the central coast of Vietnam, also varied significantly from year to year. It was demonstrated that the monsoonal forcing over the SCS, the interannual variability of which was closely associated with El Niño events, played an important role in modulating the interannual variability of the SCSWBC, whereas the influence from the upper-layer Luzon Strait transport was secondary.

Keywords South China Sea western boundary current · Features and variability · El Niño · Monsoon · Luzon Strait transport

Responsible Editor: Andy Hogg

This article is part of the Topical Collection on *the 7th International Workshop on Modeling the Ocean (IWMO) in Canberra, Australia 1–5 June 2015*

✉ Huijie Xue
hxue@maine.edu

[1] State Key Laboratory of Tropical Oceanography, South China Sea Institute of Oceanology, Chinese Academy of Sciences, Guangzhou 510301, China

[2] Graduate School, University of Chinese Academy of Sciences, Beijing 100049, China

[3] School of Marine Sciences, University of Maine, Orono, ME 04469, USA

[4] South China Sea Marine Prediction Center, State Ocean Administration, Guangzhou 510301, China

1 Introduction

As the largest marginal sea in the western Pacific Ocean, the South China Sea (SCS; Fig. 1) is characterized by a mighty current along its western boundary, namely, the South China Sea western boundary current (SCSWBC), which can reach a depth of about 600 m with a maximum instantaneous velocity of more than 1 m s^{-1} and plays a key role in the distribution of mass, energy, and heat balances in the SCS. The reviews by Fang et al. (2012) and Wang et al. (2013) highlighted the relevant research progress on the SCSWBC. Different from the western boundary currents in the open oceans, the SCSWBC has a prominent seasonality, which was revealed in the early studies by Dale (1956) and Wyrtki (1961). It is generally believed that the SCSWBC flows southward in the slope regions off China and Vietnam in winter (the blue

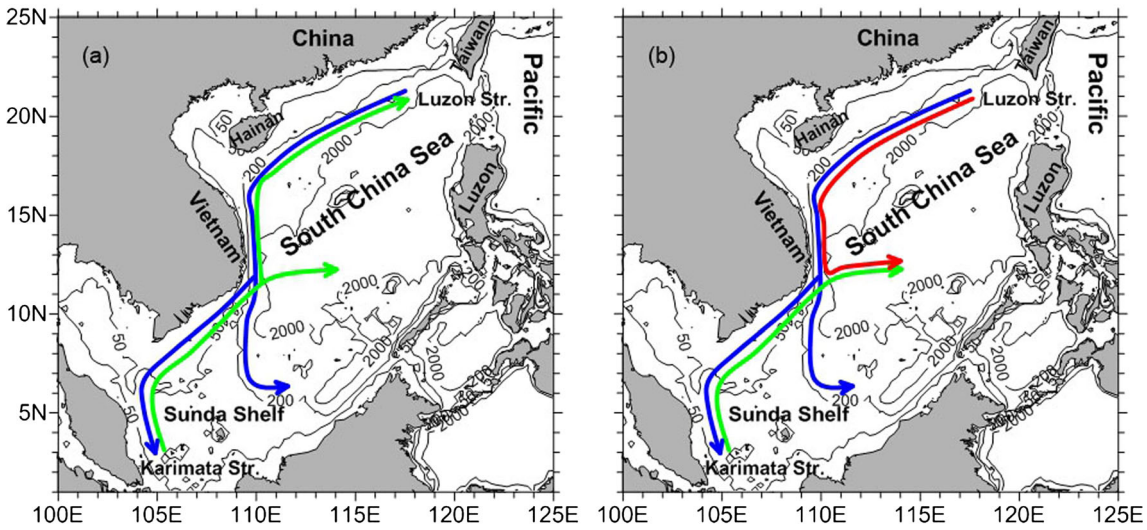

Fig. 1 Topography (m) of the SCS and the schematic of the SCSWBC. The *blue* streamline represents the SCSWBC in winter, while **a** the *green* streamline represents the SCSWBC in summer according to some studies (e.g., Shaw and Chao 1994; Chu et al. 1999; Li et al. 2000; Yang et al. 2002; Xue et al. 2004; Fang et al. 2009), and **b** the *green* and the *red* streamlines separately represent the southern and the northern branches of the SCSWBC in summer according to some other studies (e.g., Qiu et al. 1984; Huang et al. 1997; Su 2004; Wang et al. 2006a; Cai et al. 2007). The eastward streamline at about 12° N represents the VOC

streamlines in Fig. 1). When it reaches the Sunda Shelf, one part flows out of the SCS via the Karimata Strait and the other part turns northeastward to form the cyclonic circulation in the SCS (e.g., Guo et al. 1985; Fang et al. 1998; He and Wang 2007; Zhou et al. 2010). However, the summer pattern of the SCSWBC is still in dispute. In some studies (e.g., Shaw and Chao 1994; Chu et al. 1999; Li et al. 2000; Yang et al. 2002; Xue et al. 2004; Fang et al. 2009), the SCSWBC in summer is thought to flow northward from the Karimata Strait and be divided into two branches east of Vietnam (the green streamlines in Fig. 1a). The coastal branch still flows northward and joins the circulation in the northern SCS. The other branch turns eastward to form the Vietnam Offshore Current (VOC). However, in other studies (e.g., Qiu et al. 1984; Huang et al. 1997; Su 2004; Wang et al. 2006a; Cai et al. 2007), the SCSWBC in summer is thought of as two opposite-flowing branches, corresponding to a dipole circulation in the SCS. The southern branch of the SCSWBC flows northward from the Karimata Strait (the green streamline in Fig. 1b), and the northern branch flows southward along the slope of the northern SCS (the red streamline in Fig. 1b). These two branches meet each other off the southeast coast of Vietnam and then turn eastward to form the VOC.

Besides the pronounced seasonality, the SCS general circulation also exhibits considerable interannual variability (e.g., Wu et al. 1998; Wu and Chang 2005; Fang et al. 2006; Wang et al. 2006b; Chang et al. 2008; Xing et al. 2012). In these studies, the interannual variation of the SCS circulation was mainly attributed to the East Asian monsoon anomaly, which was closely associated with El Niño events via a teleconnection between the central Pacific and East Asian (Wang et al. 2000). The SCS circulation was strengthened in the El Niño developing summer but weakened in the developing winter and the decaying summer. When zooming in to the western SCS, previous studies of the interannual variability focused on the summer upwelling off the coast of Vietnam and the accompanying VOC (e.g., Xie et al. 2003; Chen and Wang 2014; Li et al. 2014), and a common conclusion was that the changes were induced by the SCS summer monsoon anomaly associated with El Niño. Similarly, the anomalous conditions of the SCSWBC near Xisha in the summer of 2010 and 2011 seen from 7 years of directly measured velocity profiles were also attributed to the basin-scale wind field anomaly associated with the 2009/2010 El Niño and 2010/2011 La Niña (Shu et al. 2016). These studies are insightful but still limited in time and space since they tended to focus on a specific part of the SCSWBC in a specific season, which was not enough to reveal the continuous variation of the entire stretch of SCSWBC during the past years. On the other hand, the Luzon Strait Transport (LST), which was considered as an oceanic connection to convey the impact of ENSO into the SCS (Qu et al. 2004, 2009), was also important to the formation of the SCSWBC (Chen and Xue 2014). Xu and Oey (2015) concluded that the wind stress curl (WSC) and the Luzon Strait intrusion account for 62 and 38 %, respectively, of the seasonal variability in the northern SCS. However, their effects on the interannual variability of the SCSWBC have not been differentiated.

Due to the lack of broad-scale, sustained in situ observations, the panorama of the SCSWBC is still not completely unveiled. The existing schematics (Fig. 1) are based mostly on geographic proximity to the side boundaries. To acquire a comprehensive understanding of the SCSWBC, a newly released regional reanalysis dataset of the SCS is analyzed in

conjunction with in situ and satellite observations. The objectives for this study are (1) to depict the main features of the SCSWBC during the past years and find out the similarities and differences with the previous studies, (2) to tease apart the dynamical origins of the currents in the northern and western SCS so that the role of local versus remote forcing as well as basin-wide dynamical adjustment can be differentiated, and (3) to determine the relative importance of the monsoonal forcing over the SCS and the remote LST forcing in driving the interannual variability of the SCSWBC. Details about the data utilized in this work are introduced in Section 2. In Section 3, main features of the SCSWBC both in summer and winter from 1992 to 2011 are portrayed. The interannual variability of the SCSWBC and its influencing factors are examined in Section 4. Finally, major conclusions are summarized in Section 5.

2 Data

The reanalysis dataset of the SCS (REDOS) presented by Zeng et al. (2014) was analyzed in this study. With an eddy-resolving horizontal resolution of 0.1° × 0.1° and 24 layers in the vertical from 0 to −1200 m, the monthly data cover the domain from 1° N to 30° N, 99° E to 134° E and the period from 1992 to 2011. Taking the global Simple Ocean Data Assimilation (SODA; Carton et al. 2000a, b) data as the open boundary forcing and assimilating a large number of observed data (particularly including multiyear temperature/salinity profiles collected annually by the South China Sea Institute of Oceanology) in the SCS and its adjacent areas, the REDOS can basically reveal the main features and variations of the physical phenomena in the SCS (Zeng et al. 2014). Variables included in the current release of REDOS are the sea surface height, 3D temperature, salinity, and horizontal velocity components.

The gridded absolute dynamic topography (ADT) and surface geostrophic velocities were obtained from the French Archiving, Validation and Interpretation of Satellite Oceanographic data (AVISO) project (Ducet et al. 2000). For the present work, the daily data, having a spatial resolution of 0.25° × 0.25° and from 1993 to 2011, were averaged to produce monthly means.

The monthly sea level from the tidal station Qui Nhon (109.3° E, 13.8° N) in Vietnam from 1993 to 2011 was also analyzed. The part between 1993 and 2006 was obtained from the Permanent Service for Mean Sea Level (PSMSL; Holgate et al. 2013) and the other part between 19 October 2007 and 31 December 2011 with about 60 % completeness was from the University of Hawaii Sea Level Center (UHSLC). We used the regression method to fill the missing data with the following equation:

$$SL_{TG} = 0.904 \times SL_{AVISO} + 0.107, \quad (1)$$

where SL_{TG} and SL_{AVISO} represent the concurrent sea level from the tide-gauge and from the AVISO data extrapolated to the Qui Nhon station, respectively. SL_{TG} and SL_{AVISO} are highly coherent with a correlation coefficient of 0.87 (over 95 % confidence level).

The monthly mean surface wind from the cross-calibrated multi-platform (CCMP; Atlas et al. 2011) was adopted in this paper. Similar to the AVISO ADT, the CCMP wind product has a horizontal resolution of 0.25° × 0.25° and covers the same period from 1993 to 2011. It should be noted that the REDOS was driven by the CCMP wind and assimilated the AVISO data.

3 Main features of the SCSWBC from 1992 to 2011

3.1 Definition of the SCSWBC in this study

The traditional definition of the SCSWBC reviewed in the introduction tended to include all the currents along the western boundary of the SCS regardless of their differences in dynamics. Using the CCMP wind data, the monthly wind stress over the SCS from 1993 to 2011 was calculated following Large et al. (1994) and the monthly WSC was then obtained. We calculated the vector correlation (Crosby et al. 1993) between the local wind stress and the top 200-m mean velocity from the REDOS. The currents on the southwestern shelf and the northern shelf east of the Pearl River estuary are closely related to the local wind stress, while the currents along the northern and the western slopes are not (Fig. 2).

On the other hand, the transport in the interior ocean driven by the basin-wide WSC should be balanced by the strong return flow along the western boundary following the

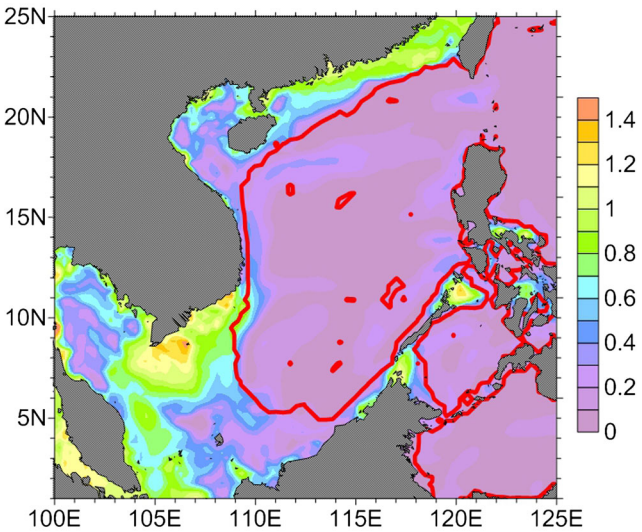

Fig. 2 Vector correlation (*shading*) between the local wind stress and the top 200-m mean velocity. The *red line* denotes the 200-m isobath

westward intensification theory of Stommel (1948). To qualitatively figure out the correspondence between the basin-wide wind forcing and the currents along the northern and western slopes in the SCS, the Sverdrup (1947) transport stream function as

$$\psi(x) = -\frac{1}{\rho\beta}\int_{x}^{x_E} \mathrm{curl}(\tau)\mathrm{d}x \qquad (2)$$

was calculated in the deep basin where the water depth is greater than 1000 m and compared with the climatological upper-layer SCS circulation from the REDOS. Here $\Psi(x)$ is the stream function, $\rho = 1.025 \times 10^3$ kg m^{-3} is a reference density of seawater, $\beta = 2 \times 10^{-11}$ m^{-1} s^{-1} is the northward gradient of the planetary vorticity, curl(τ) is the climatological WSC, and x_E is the eastern boundary at which $\Psi = 0$. It was found that the stream function patterns are in good agreement with the top 200-m averaged circulation from the REDOS (Fig. 3). For the summer case, the WBC in the northern SCS flows along the slope and is rather consistent with the stream function in the northern half of the deep basin. However, the so-called southern branch of the SCSWBC in traditional definition mainly exists on the southwestern shelf and does not match the stream function in the southern deep basin. As to the case in winter, the SCSWBC stretches to a full length along the western slope, but it appears to be associated with two separate cyclonic gyres on the eastern side and in the interior of the basin. The overall winter circulation agrees rather well with the Sverdrup stream function in the deep basin.

Solely based on the responses to wind forcing, the vector correlation and the Sverdrup stream function analysis presented above indicate that the currents on the southwestern shelf are driven by the local wind stress directly, which are usually classified as the wind-driven coastal currents (the green solid streamline in Fig. 4), while the currents along the northern and western slopes seem to be closely associated with the basin-wide WSC, which are similar to the WBCs (e.g., the Kuroshio and the Gulf Stream) in the open oceans. Therefore, only the southwestward and the southward currents along the northern and western slopes were defined as the SCSWBC in the present work. The corresponding schematics of the SCSWBC in winter and summer are shown in Fig. 4 in blue and red, respectively. The main features and variability of the SCSWBC were examined in the following sections.

3.2 The SCSWBC in winter

The SCSWBC in winter was calculated as the 3-month mean from December, January, and February (DJF) of the following year. Figure 5 shows the SCSWBC in each winter of 1992–2011. Note that winter 2011 was the monthly mean of December only. Based on the 20-year REDOS data, in winter, the SCSWBC flowed southwestward along the slope of the northern SCS, then turned southward in the vicinity of Hainan Island and extended the full length of the western slope, and finally turned northeastward joining the cyclonic circulation (the blue streamline in Fig. 4). The maximum velocity of the SCSWBC usually appeared off the southeast coast of Vietnam.

For the wintertime SCSWBC, the most unstable segment was located in the slope region of the northern SCS, the axis of which meandered with a meridional swing. For example, there was a deviation of about 1° between 1999 and 2001 by taking the 500-m isobath in Fig. 5 as the reference. The segment along the coast of Vietnam was relatively steady except for its width (between 109.5° E and 111° E on average). During El Niño events, the SCSWBC tended to be weakened in winter of the developing phase, such as in 1994, 1997, 2002, 2004, 2006, and 2009 (highlighted in blue in Fig. 5), whereas

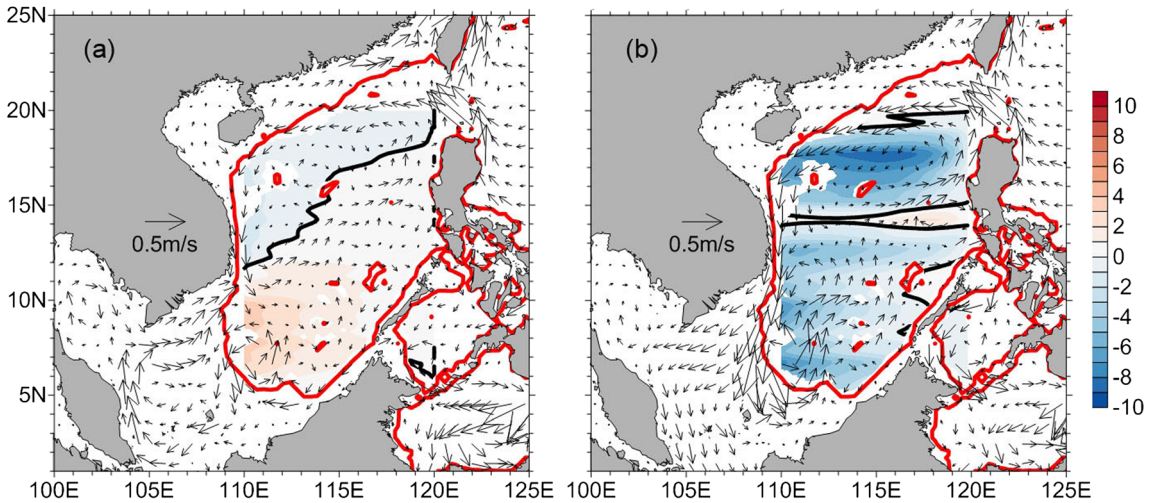

Fig. 3 Climatological Sverdrup stream function (*shading*; Sv) in the SCS basin deeper than 1000 m and the top 200-m mean velocity (vectors; m s^{-1}) from the REDOS for **a** summer and **b** winter, respectively. The *black line* is the zero contour and the *red line* denotes the 200-m isobath

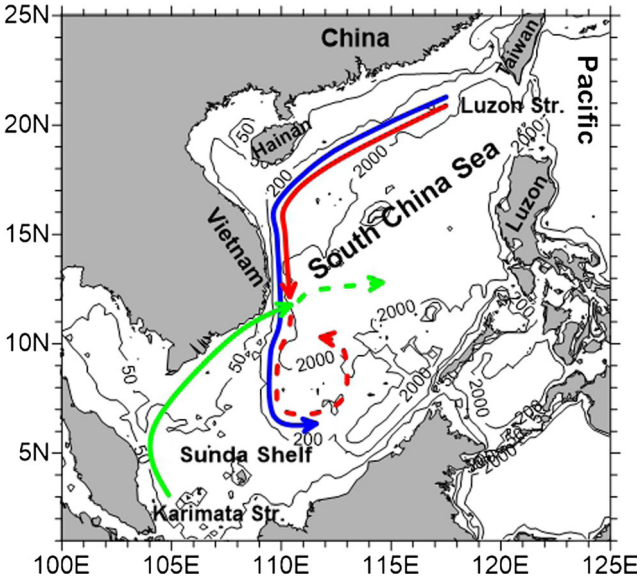

Fig. 4 Schematic of the SCSWBC based on the definition in this paper. The *blue* streamline denotes the SCSWBC in winter. The *red solid* streamline represents the SCSWBC in summer, and the *red dashed* streamline denotes the extension of the WBC which sometimes forms a cyclonic gyre. The *green solid* streamline denotes the current from the southwestern shelf, and the *green dashed* streamline represents the VOC in summer

it was intensified in the following winter, such as in 1995, 1998, 2003, 2005, 2007, and 2010 (highlighted in red in Fig. 5).

3.3 The SCSWBC in summer

The SCSWBC in summer defined as the 3-month mean from June, July, and August (JJA) tended to be much more complicated than the winter pattern (Fig. 6). In the northern SCS, the WBC generally followed the same path of the winter but became weaker (the red solid streamline in Fig. 4). Fang et al. (2012) thought that this southwestward segment of the WBC basically appeared as a subsurface current, but according to the REDOS, it also extended to the surface and was often perturbed by eddies. As a result, it was not easy to identify the flow path, especially in 1998, 1999, 2007, and 2009. In the southern SCS, a broad current came from the Karimata Strait and flowed northeastward along the coast of Vietnam, which merged with the southward SCSWBC to form the VOC (the green dashed streamline in Fig. 4). The existence of VOC was attributed to WSC (Chu et al. 1998, 1999; Shaw et al. 1999; Liu et al. 2001b; Cai et al. 2005, 2007), which could then be a part of the SCSWBC. On the other hand, Gan et al. (2006) and Gan and Qu (2008) suggested that the interaction between the wind-driven coastal jet and the bottom topography controls the VOC. The VOC is also likely affected by mesoscale eddies since the eddy kinetic energy is very strong off the Vietnam coast (Wang et al. 2012).

The axis of the VOC was identified as the maximum of the eastward velocity between 10° N and 15° N, and its mean latitude was at about 12° N. The VOC moved more northward in 1995 and 1998 (highlighted in red in Fig. 6), when the southward SCSWBC retreated. Moreover, an extreme event occurred in 2010. In the summer of that year, an exceptional anticyclonic eddy formed in the area southeast of the Hainan Island (Chu et al. 2014). As a result, the currents along the coast of Vietnam flowed northward and the VOC totally disappeared. But in some other years (e.g., 1994, 1997, 2002, 2004, and 2011; highlighted in blue in Fig. 6), the SCSWBC became more powerful and pushed the VOC further south. Nevertheless, the southward shifts (about 1°) were weaker than the northward ones (about 2~3°).

On the continental slope, flows were generally southward associated with a cyclonic eddy in the southwest corner of the deep SCS basin (the red dashed streamline in Fig. 4), which can be found even in the 500-m layer (not shown). This cyclonic eddy might be overestimated by the REDOS since it was reported only in subsurface layers (Xu et al. 1982; Chu and Li 2000; Fang et al. 2002). Although the cyclonic eddy does not agree with the Sverdrup stream function (Fig. 3a), the correlation map (Fig. 7) suggests that the cyclonic eddy had a close tie to the SCSWBC north of the VOC. It seemed plausible to consider the southward flows on the slope as an extension (or southern branch) of the SCSWBC when the cyclonic eddy occurred.

4 Interannual variability of the SCSWBC from 1992 to 2011

4.1 SCSWBC transport off the coast of Vietnam

To estimate the SCSWBC transport, a zonal transect located at 13.8° N and spanning from 109.5° E to 112° E, corresponding to the location of Qui Nhon, was selected for analysis (Fig. 7). By calculating the correlation coefficient of the top 200-m mean velocity magnitude between the SCSWBC axis (109.75° E, 13.8° N; max velocity axis based on Figs. 5 and 6) at the transect and the other places in the entire SCS, the values more than 0.3 with confidence level exceeding 95 % assembled almost inclusively in the region of the SCSWBC, implying that the SCSWBC at this transect could be a good representation of its features and variations. As such, yearly distributions of the SCSWBC at this section, both for the winter and summer, were shown in Figs. 8 and 9, respectively. The SCSWBC exhibited as a jet in the upper slope region from the surface down to about 600 m with an opposite flow (i.e., northward flow) below. This is consistent with the top two layers of the three-layer SCS circulations as described in Wang et al. (2011) and Shu et al. (2014) such that the circulation is cyclonic in the surface layer but anticyclonic in the

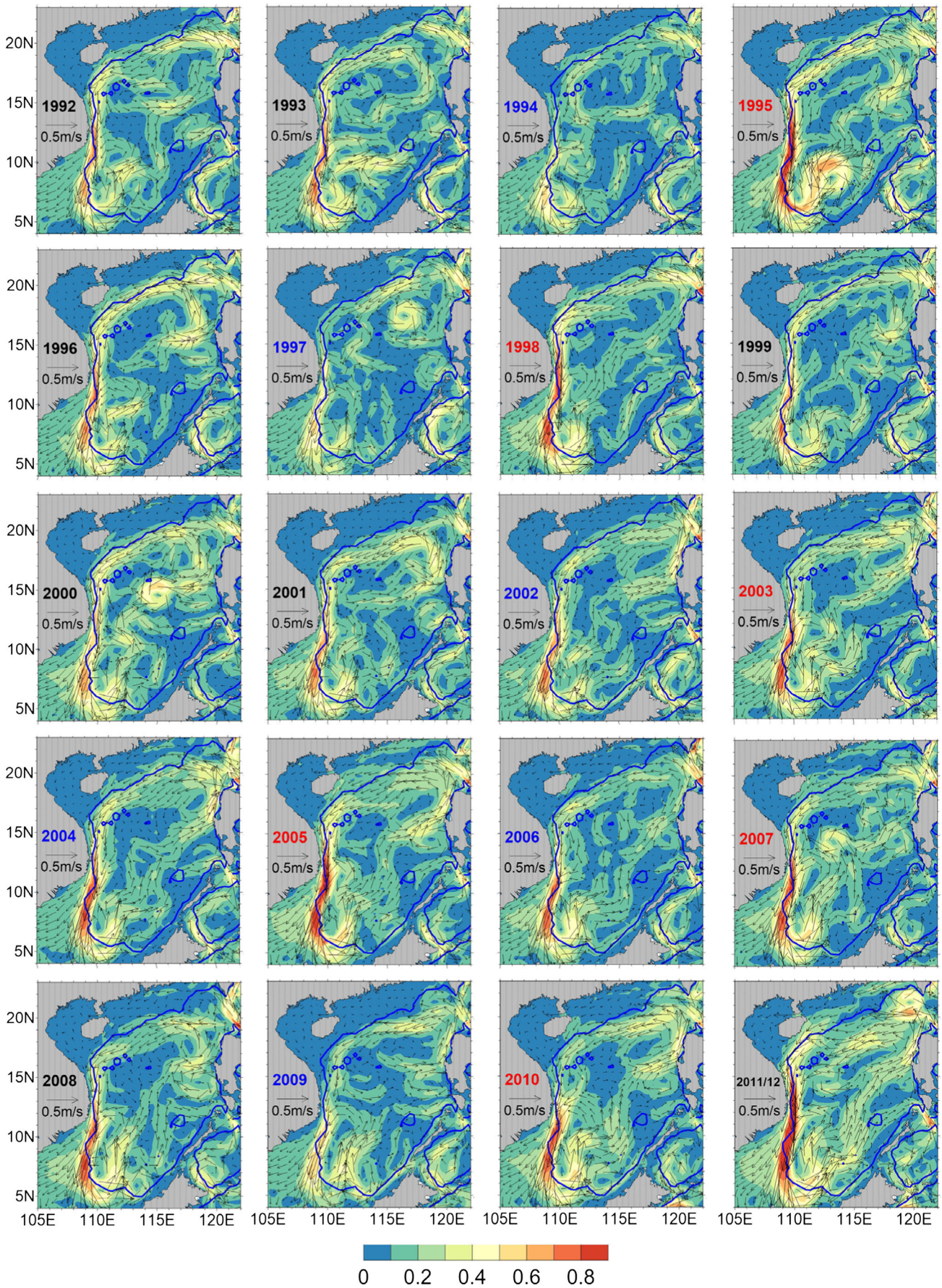
1992
1993
1994
1995
1996
1997
1998
1999
2000
2001
2002
2003
2004
2005
2006
2007
2008
2009
2010
2011/12
0.5m/s
20N
15N
10N
5N
105E
110E
115E
120E
0
0.2
0.4
0.6
0.8

◀ **Fig. 5** Winter (DJF) mean upper-layer (top 200 m) circulation (vectors) and velocity magnitude (*color shading*; m s^{-1}) from 1992 to 2011 in the SCS. *Blue solid line* is the 500-m isobath. The years with a weakened (intensified) SCSWBC during the growing (decaying) phase of an El Niño event were highlighted in *blue* (*red*)

middle layer. The current axis was roughly along the 500-m isobath. Similar to many boundary currents, the core of the current shifted offshore with the depth of the jet. The current was stronger in winter than in summer. Although there were large year-to-year differences, the SCSWBC was generally wider but shallower in winter than in summer.

To obtain a quantitative description of the SCSWBC at this transect, the longitude of the maximum velocity located between the surface and 200-m depth was defined as the longitude of the axis. Moreover, the contour of −0.1 m s^{-1} instead of zero was taken to identify the boundary of the SCSWBC due to the uncertainty associated with the latter. Indices such as the axis, depth, and width of the SCSWBC were extracted from Figs. 8 to 9, and their time sequences, mean values, and standard deviations were shown in Fig. 10. In winter (blue lines in Fig. 10), the SCSWBC axis was located at 109.75° E on average with a standard deviation of 0.07°, being closer to the coast in most of the El Niño winters (1994, 1997, 2002, and 2006). The mean depth and width of the wintertime SCSWBC were −559.08 ± 160.27 m and 190.1 ± 49.7 km, respectively. In some El Niño winters (1994, 2002, and 2009), the SCSWBC was deeper than that in the following winters, but the situation reversed in some other winters (1997, 2004, and 2006). For the width of the SCSWBC, it was narrower in most of the El Niño winters than in the following winters.

In summer (red lines in Fig. 10), the SCSWBC axis was only slightly further from the coast (located at 109.77 ± 0.10° E). With a larger standard deviation, the summertime SCSWBC deepened to −650.18 ± 201.37 m and narrowed to 166.3 ± 68.0 km, suggesting a more notable interannual variation than that in winter. In most of the El Niño decaying summers (1995, 1998, and 2005), the SCSWBC tended to become deeper and wider than that in the developing summers. However, in the summers of 2007 and 2010 when the El Niño decayed, the southward SCSWBC was broken or even reversed by eddies (Fig. 6), resulting in a shallower and narrower SCSWBC at this transect (Figs. 9 and 10). In addition, the SCSWBC tended to be narrower than the mean from 1993 to 1999, then became wider from 2001 to 2005 and narrowed again since 2006, suggesting a longer period of modulation for the interannual variability of its width.

Considering that there are very few velocity measurements of the SCSWBC, the sea level data that are more readily available may be utilized to estimate the long-term SCSWBC transport by establishing a regression relationship between the transport and the simultaneous sea level difference (SLD) across the SCSWBC. Similar approaches have been successfully applied to the Kuroshio and Ryukyu Current by Imawaki et al. (2001), Zhu et al. (2004), and Andres et al. (2008). Since it was difficult to identify the boundary of the SCSWBC in real time, the SLD between 109.5° E and 111° E (the mean position of the offshore boundary at 13.8° N) was used. Within the same gap, the dominant transport above the depth of the SCSWBC (or 600 m whichever is smaller) was integrated. According to our definition, only the negative transport was taken as the SCSWBC transport. The positive transport occurred when the northward current from the south occupied the gap. The method above ensured the SLD and the transport basically consistent with each other to establish their regression relationship later. The root-mean-square error in the estimated transport induced by ignoring the changes in the width and depth of the SCSWBC was 3.3 Sv, much smaller than the peak-to-peak range of the time series at about 50 Sv. By comparing with the results (not shown) based on the ocean general circulation model for the Earth Simulator (OFES—http://www.jamstec.go.jp/esc/research/AtmOcn/product/ofes.html), which is a near-global model without data assimilation (Masumoto et al. 2004), both the REDOS' SLD and the direction of the transport are closer to the SLD and the surface geostrophic velocity derived from AVISO (Fig. 11), with a correlation coefficient of 0.88 and 0.75 (0.72 and 0.50 for the OFES results, all above 95 % confidence level), respectively. Similar to other large-scale currents with a quasigeostrophic property (e.g., the Kuroshio, see Chang and Oey 2011), there is a high correlation coefficient of 0.88 with a 95 % confidence level between the calculated transport and SLD from the REDOS data. Thus, following the methods by Imawaki et al. (2001), a regression equation based on the REDOS results was established as

$$\mathrm{Trsp} = 61.55 \times \Delta\eta - 2.58, \tag{3}$$

where $\Delta\eta$ is the SLD and Trsp is the transport. The regressed transports were in good agreement with the direct estimations from the REDOS. Their root-mean-square deviation (RMSD) is 4.65 Sv, much smaller than the peak-to-peak range of about 50 Sv.

To link the transport with observations, it is desirable to introduce the measured SLD into the estimation. Satellite altimeter data at (109.5° E, 13.8° N) and (111° E, 13.8° N) were employed in one estimate, whereas tide-gauge data from the station Qui Nhon (109.3° E, 13.8° N) on the shore replaced the altimeter data at (109.5° E, 13.8° N) in another estimate to avoid the inherent error of altimeter data near shore. Since the station is only about 20 km from the western end of the transect (see Fig. 7) and within the distance gap the water depth is shallower than 100 m, the volume transport through the gap is expected to be much smaller than that of the main body of the SCSWBC. By unifying the two types of data with common references of mean sea level, the observed SLD

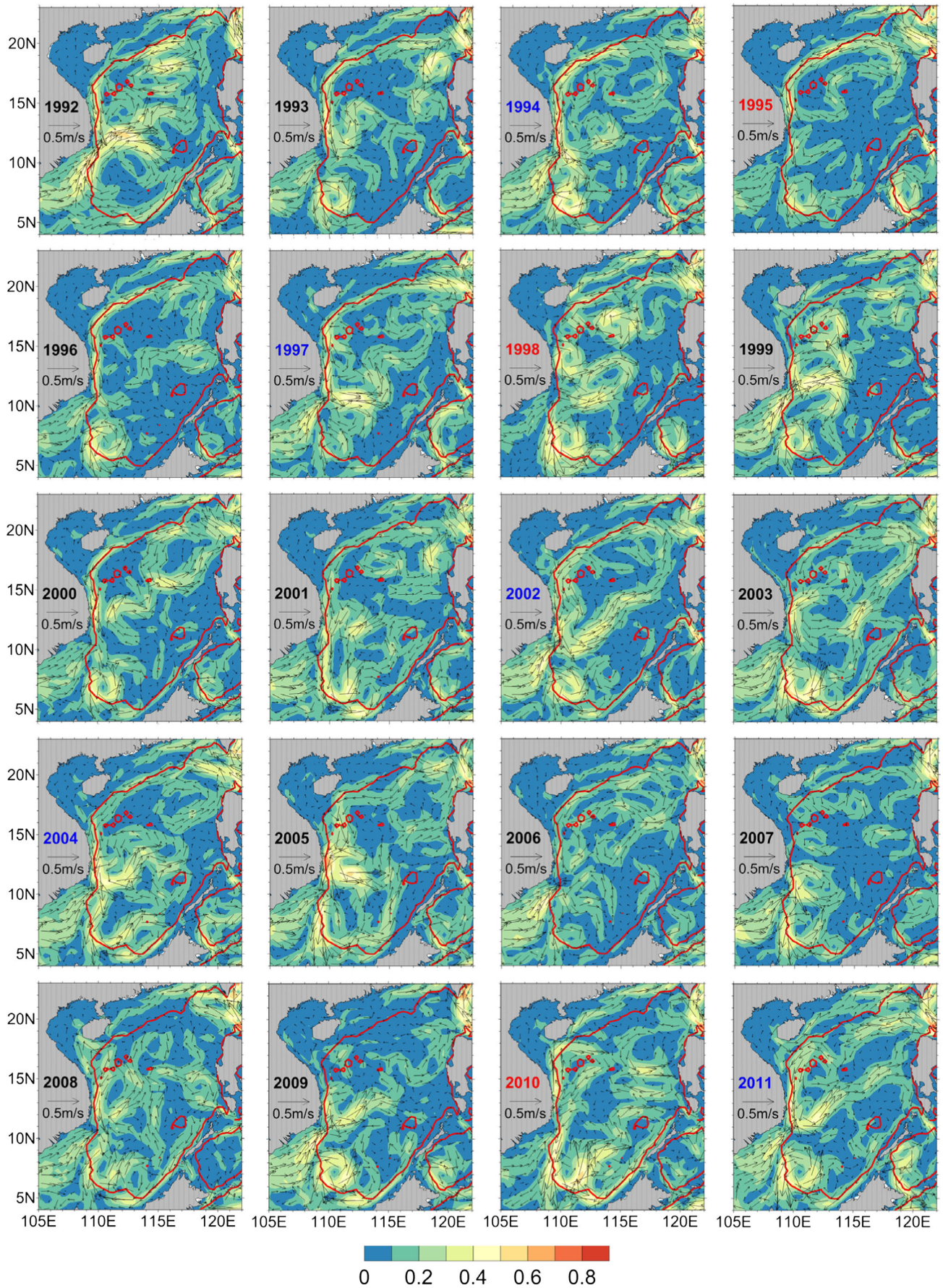
1992
1993
1994
1995
1996
1997
1998
1999
2000
2001
2002
2003
2004
2005
2006
2007
2008
2009
2010
2011
0.5m/s
20N
15N
10N
5N
105E
110E
115E
120E
0
0.2
0.4
0.6
0.8

◀ **Fig. 6** Similar to Fig. 5 but for the summer (JJA) mean upper-layer circulation. *Red solid line* is the 500-m isobath. The years with a northward (southward) shift of the VOC were highlighted in *red* (*blue*)

between the two stations were then calculated (the red line in Fig. 11a), which could be compared with the SLD based on only the AVISO data (the green line in Fig. 11a). The three SLDs agreed with each other for both the original time series shown in Fig. 11a and their anomalies, but the differences were generally larger in summer than in winter, particularly for the summers of 1993, 1995, 1996, 1998, 2005, and 2008.

The modified transports (the red and green lines in Fig. 11b) were then obtained by substituting the SLDs into Eq. 3. The winter (DJF) mean of the SLD-based SCSWBC transport was −11.8 ± 3.5 Sv (−13.0 ± 3.1 Sv for the SLD based on the AVISO data only and −13.6 ± 3.6 Sv from the REDOS; 1 Sv = 10^6 m^3 s^{-1}), which is comparable to the estimation of −10.6 Sv by Chu et al. (1999) but larger than the value of −5 Sv by Wyrtki (1961). However, the SLD-based southward transports in summer were generally weaker than the direct estimations from REDOS (the blue line in Fig. 11b). Moreover, for the summers of 1993, 1996, 1998, and 2008, the SLD-based transports even reversed to become northward, and for the summers of 1995 and 2005, the calculated northward transports based on Eq. 3 were considerably stronger than those based on the REDOS data. These large uncertainties for the SLD-based estimations in summer could be related to the 13.8° N section being near the location where the southward SCSWBC met the northward flows from the southwestern shelf. The positive transports appeared when the northward currents from the south occupied this section.

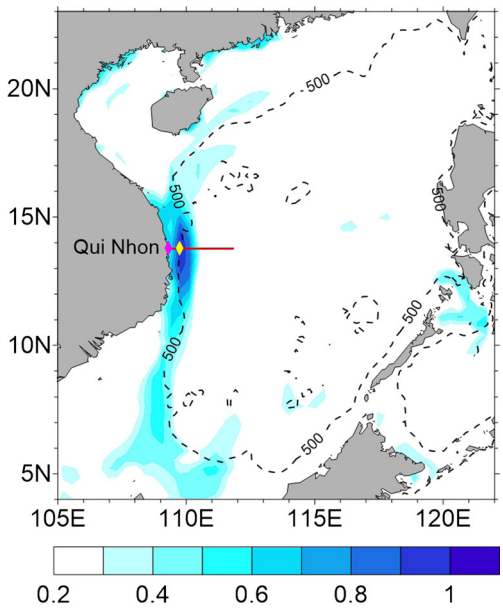

Fig. 7 Transect off the coast of Vietnam (*red solid line*) and map of the correlation coefficient of the upper-layer velocity magnitude (vertical mean in the top 200 m) between the SCSWBC axis (109.75° E, 13.8° N; marked by the *yellow diamond*) at the transect and other locations in the SCS (*color shading*). Areas with insignificant correlation (correlation coefficient <0.3) were masked. The Qui Nhon station (109.3° E, 13.8° N) was marked by the *magenta diamond*. *Dashed line* represents the 500-m isobath

Actually, the maximum probability density function of the SLD-based transports at this transect was −1.9 Sv in summer, whereas the mean value is 1 Sv with a considerable standard deviation of 6.3 Sv (0.6 ± 6.3 Sv for the SLD based on the AVISO data only and −4.6 ± 6.6 Sv from the REDOS), which was biased due to much larger positive anomalies in some years after incorporating the SLD from AVISO and in situ observations in Eq. 3. These results suggest that there might be some deficiencies for using the REDOS to deduce the transport at this location during several questionable summers, which corresponded directly with the contemporaneous deviations of the REDOS' SLD from the observations as seen in Fig. 11a. Note that the positive values in the time series did not represent the SCSWBC transports, but they signaled the anomalous conditions of the SCSWBC indirectly since the southward SCSWBC can reach this transect in most cases. Hence, if only the southward SLD-based transports were taken for statistics, the summer (JJA) mean SCSWBC transport was −3.0 Sv with a standard deviation of 1.6 Sv when both the AVISO and tide-gauge data were used to obtain the regressed transport.

Zhu et al. (2015) developed a similar regression relationship between the transport derived based on 22-month continuous observations from 5 pressure-recording inverted echo sounders (PIES) and concurrent satellite SLD for a transect across the slope southeast of the Hainan Island, which was then used to estimate the transport between 1992 and 2014 by taking the advantage of extended period of satellite altimetry. The winter mean SCSWBC transport obtained in Zhu et al. (2015) was −5.1 Sv southwestward, consistent in direction but significantly smaller in magnitude than our estimate of −11.8 Sv. However, the summer mean SCSWBC transport based on their estimation was northeastward at 2.3 Sv, which was opposite in direction to our estimation of −3.0 Sv. Note that from the REDOS summertime flow fields (Fig. 6), there was a northeastward current in the shelf close to the southwestward current on the slope, but the observations by Zhu et al. (2015) showed that this northeastward current occupied the slope region on 1 July 2013, suggesting that there might be some deficiencies for the REDOS to accurately depict the relative position of these two opposite-flowing currents in this area, which could result in the discrepancy between the transport estimations. Moreover, according to Fig. 7 in their article, the differences between the transports based on the regression relationship and the direct observations were obvious. Some negative transport values changed sign after introducing the satellite SLD into the empirical relationship, which tended to affect the climatological mean value. This could be another reason for the differences between their

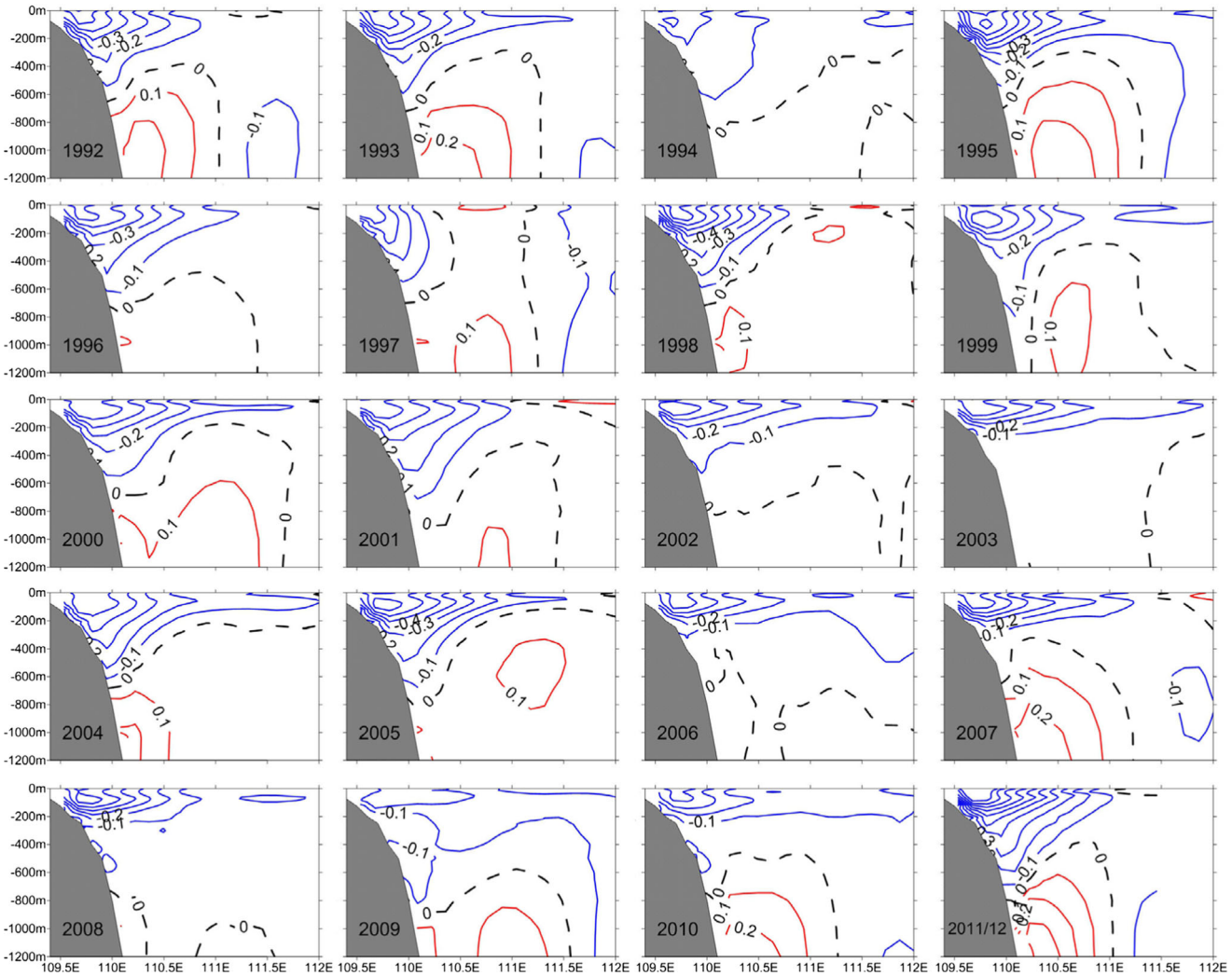

Fig. 8 Vertical sections of the winter mean meridional velocity along 13.8° N from 1992 to 2011. Negative (positive) values represent the southward (northward) currents. Contour interval = 0.1 m s^{-1}

estimate and ours. In addition, such quantitative discrepancies are understandable because of the difference in space for the estimations as evidenced by the complex spatial variations seen in Figs. 5 and 6.

4.2 Impact of the monsoon on the interannual variability of the SCSWBC transport

Based on the Sverdrup relation, the wind-driven circulation was proven to be critical for the formation of the upper oceanic circulation in the SCS (Liu et al. 2001a). As the most important part of the SCS circulation, the SCSWBC is therefore closely associated with the monsoon prevailing over the SCS, which was qualitatively revealed in Fig. 3 for the seasonal variations. Regarding the interannual time scale, the annual and decadal signals of the WSC anomaly (WSCA) were removed via a bandpass filter between 14 and 90 months. The empirical orthogonal function (EOF) analysis was performed on the filtered WSCA. The first two dominant modes, which account for 50 and 16 % of the total variance, respectively, are shown in Fig. 12. The spatial patterns of these modes (Fig. 12a, b) were similar to the typical distributions of the WSCA for winter and summer separately (not shown). Moreover, both of the principal components (PCs; the red line for PC1 and the green line for PC2 in Fig. 12c) are closely correlated to Nino3.4 index (shaded in Fig. 12c), with a maximum correlation coefficient of 0.75 for PC1 and −0.38 for PC2 (more than 95 % confidence level) at a 2- and 3-month lag, respectively. Meanwhile, there is also a statistically significant (more than 95 % confidence level) correlation coefficient of 0.41 and −0.35 between the filtered SCSWBC transport (the blue line in Fig. 12c) and the dominant modes of the basin-wide WSCA, respectively, with the filtered SCSWBC transport lagging behind the WSCA modes for 2 months.

Although we sought out the interannual time scale, the strongest signal for the wind over the SCS was still at the

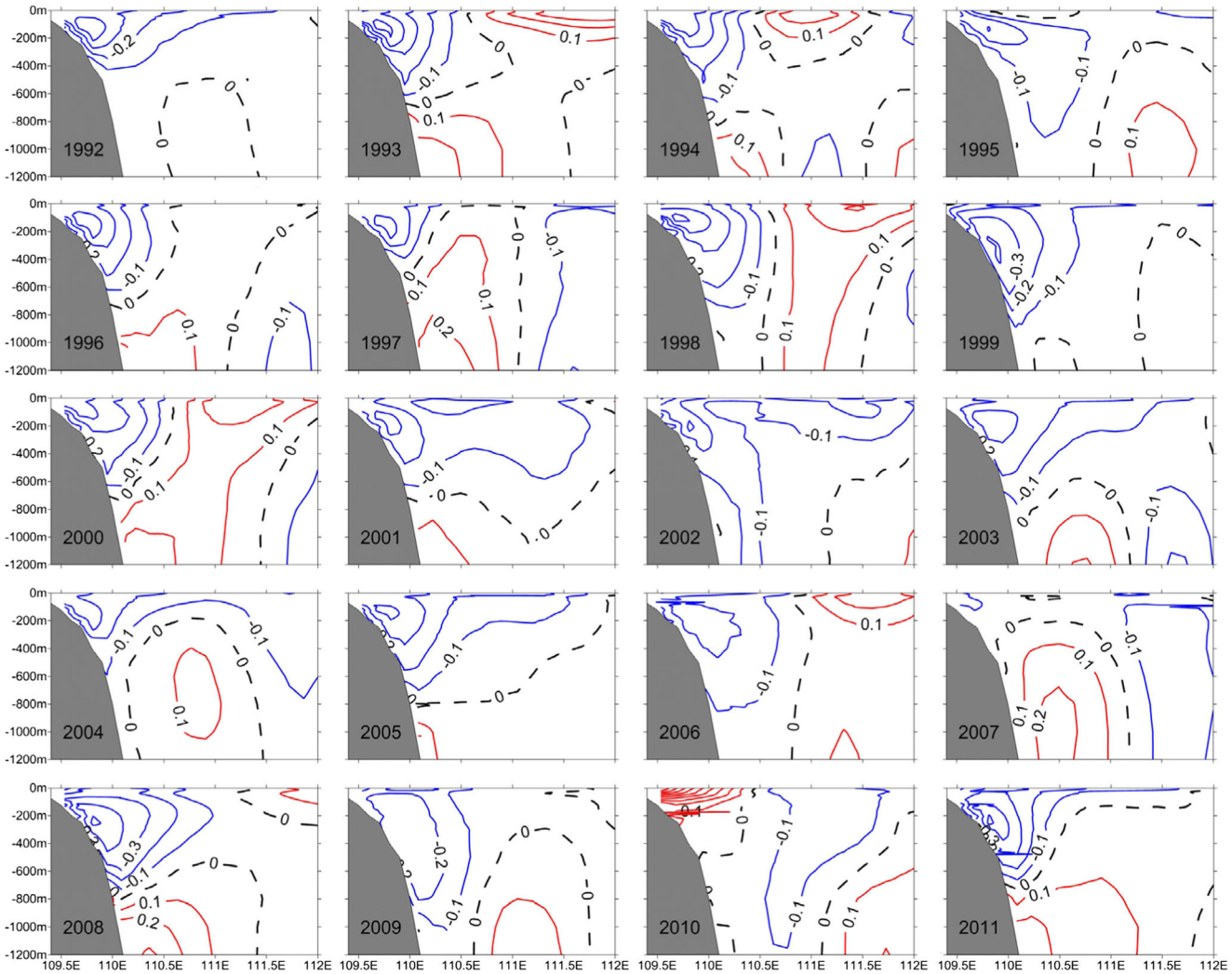

Fig. 9 Similar to Fig. 8 but for the summer-mean meridional velocity along 13.8° N

seasonal time scale (not shown). The interannual anomaly of the wind acted as a modulation to the seasonal characteristics, for example, resulting in a weaker winter monsoon over the SCS during the developing phase of El Niño. The abnormal monsoon over the SCS further induced an abnormal transport in the interior basin of the SCS, which was balanced by an

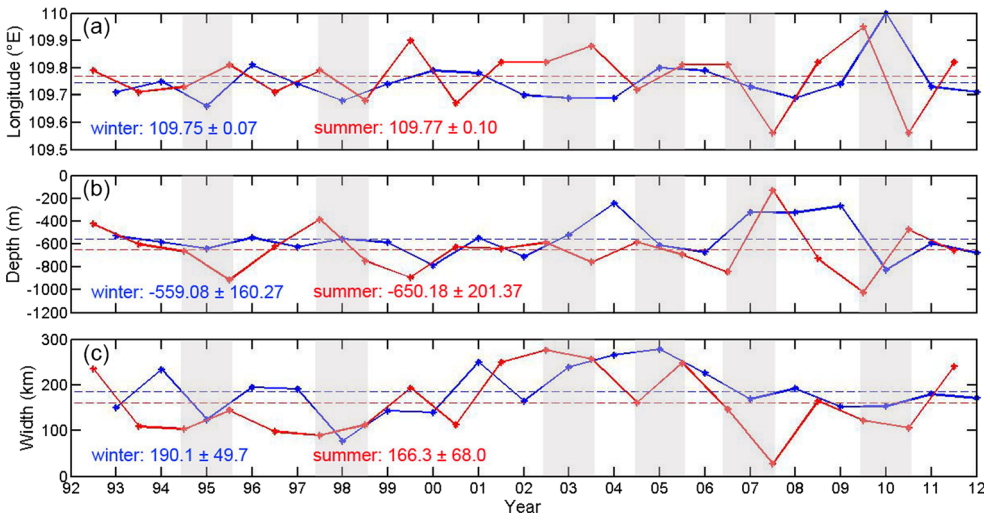

Fig. 10 Time series of **a** the axis, **b** depth, and **c** width of the SCSWBC for winter (*blue*) and summer (*red*), respectively. Mean values and standard deviations of the indices for winter and summer were listed in corresponding color. *Dashed lines* represent the mean values. All the El Niño events included in the period were *shaded* from the developing summer to the decaying summer

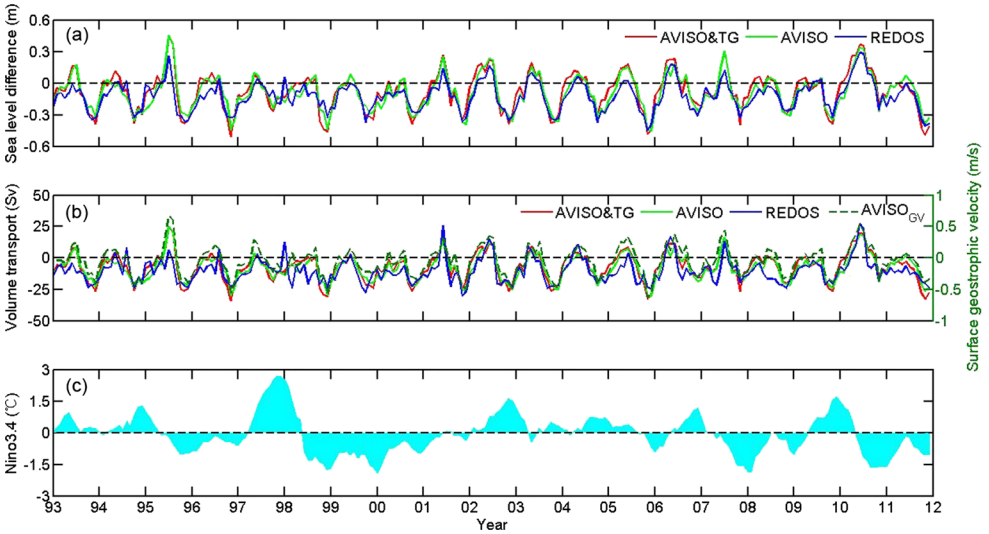

Fig. 11 **a** Time series of the SLD between 109.5° E and 111° E based on the combination of the AVISO data and the tide-gauge (*TG*) data (*red*), only the AVISO data (*green*), and the REDOS data (*blue*). **b** Time series of the dominant transport above 600 m through the same gap based on the REDOS data (*blue*), the regression equation with the combination of the AVISO data and the TG data (*red*) and with only the AVISO data (*green*), and the surface geostrophic velocity based on the AVISO data (*dark green*). Only the negative transport value was taken as the SCSWBC transport. **c** Time series of the Nino3.4 index

abnormal SCSWBC transport. Hence, the results above can be explained as follows. The basin-wide WSCA weakened when the value of PC1 was positive in winter during the developing phase of El Niño events in 1994, 1997, 2004, 2006, and 2009. Correspondingly, the southward SCSWBC transport was reduced by about 20 % with a positive anomaly. By contrast, the basin-wide WSCA was intensified when the PC1 became negative in the following winter, such as 1995, 1998, 2005, 2007

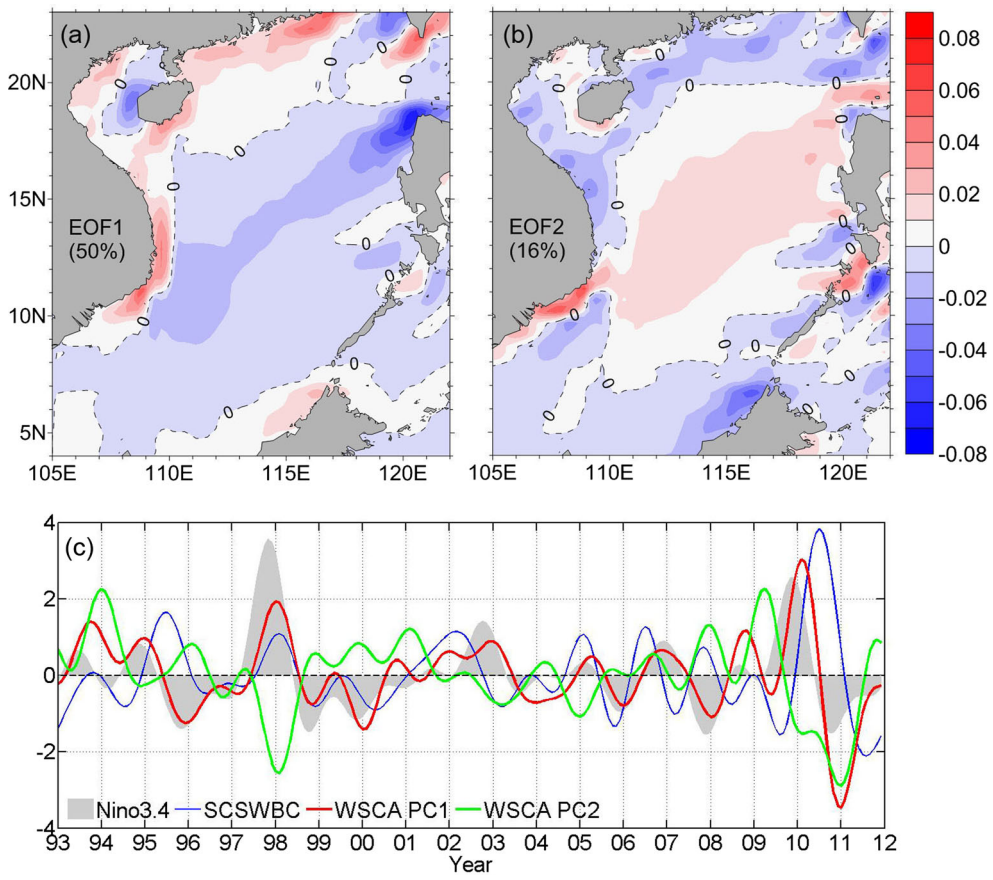

Fig. 12 **a** First and **b** second EOF modes of the WSCA (10^{-7} Nm^{-3}) over the SCS. *Dashed line* represents the zero contour. **c** Their corresponding PCs (PC1 in *red* and PC2 in *green*) with the band-passed SCSWBC transport (*blue*) and the Nino3.4 index (*shaded*). All time series were normalized by subtracting their mean value and then being divided by their standard deviation

and 2010. As a result, the southward SCSWBC transport increased by about 18 % with a negative anomaly. With respect to the case in summer, since the EOF2 had the same sign with the seasonal pattern, the basin-wide WSCA was attenuated with a negative value of the PC2 in the El Niño decaying summer, such as 1995, 1998, and 2010. Subsequently, the SCSWBC transport decreased with a positive anomaly. All of these results imply that the interannual variability of the monsoon over the SCS, which is closely correlated to the El Niño events, can modulate the interannual variability of the SCSWBC transport significantly.

4.3 Impact of the LST on the interannual variability of the SCSWBC transport

The ideal experiments conducted by Chen and Xue (2014) suggested that flows through the open straits are of equal importance compared to the monsoon for the formation of the SCSWBC. As the strongest inflow into the SCS, the LST should have a significant effect on the SCSWBC. Although produced by a regional model, the REDOS adopted the global SODA product as its open boundary forcing and assimilated a great number of observed data in the Luzon Strait and the western Pacific. As a result, the REDOS is able to capture the primary structure and variability of the flow in the Luzon Strait. Figure 13a displays the spatial structure of the 20-year mean zonal velocity from the REDOS along the section located at 120.75° E. In the upper layer above 600 m, the Kuroshio intruded into the SCS from an extensive area south of 21° N and then flowed out from the north, resulting in a net westward transport into the SCS. On the contrary, in the intermediate layer between 600 and 1200 m, even though it was weak, the flow was eastward. This vertical pattern with a net westward transport in the upper layer and a net eastward transport in the intermediate layer is generally consistent with the previous studies (Wyrtki 1961; Chu and Li 2000; Qu 2000; Qu et al. 2000; Yaremchuk and Qu 2004; Tian et al. 2006; Yuan et al. 2008; Yang et al. 2010; Zhang et al. 2015). To be consistent with the SCSWBC, only the upper-layer LST (ULST; above 600 m) through this section was calculated. Despite generally higher estimates −8.3 ± 3.4 Sv for REDOS (vis-a-vis −4.1 ± 2.3 Sv for OFES and 3.2 ± 2.7 Sv for SODA), the ULST from the REDOS exhibited variations generally consistent with the results based on OFES and SODA (Fig. 13b), and the correlation coefficients were both greater than 0.5 and exceeded 95 % confidence level.

By calculating the correlation coefficient between the band-passed ULST and the top 200-m mean velocity magnitude in each grid of the SCS, the significant values followed the path of the SCSWBC and were negative (Fig. 14), implying that the SCSWBC was intensified

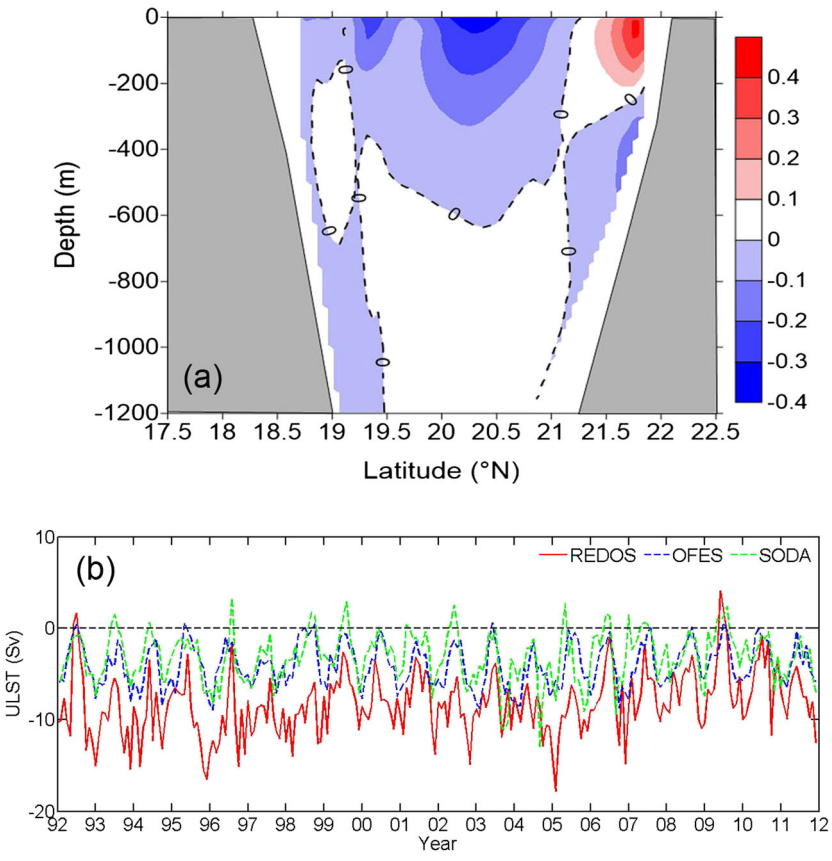

Fig. 13 **a** Spatial structure of the 20-year mean zonal velocity (m s^{-1}) along 120.75° E based on the REDOS. *Dashed line* represents the zero contour. Negative (positive) values represent the westward (eastward) currents. **b** Monthly ULST based on the REDOS (*red solid line*), OFES (*blue dashed line*), and SODA (*green dashed line*), respectively

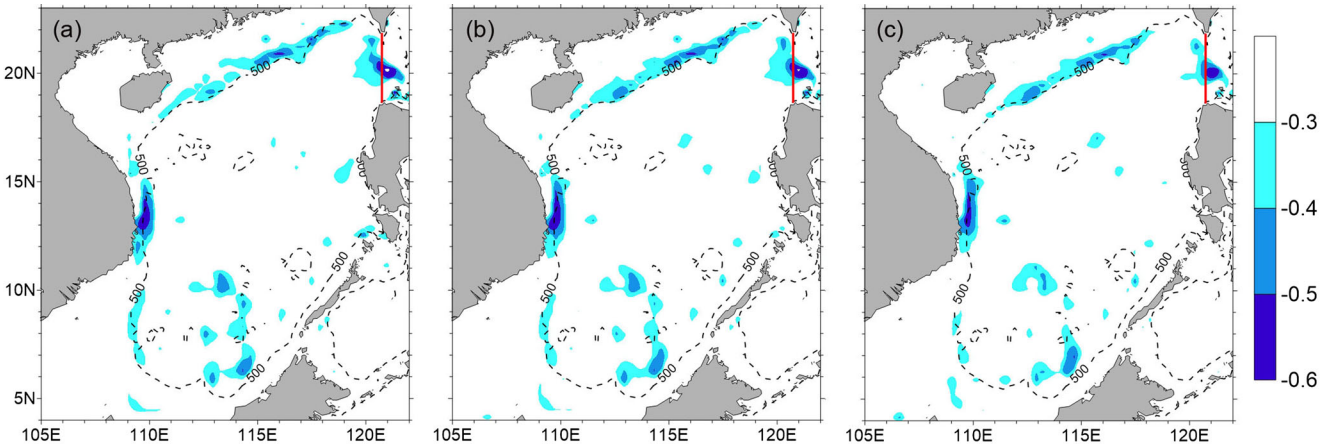

Fig. 14 Similar to Fig. 7 but for the band-passed ULST at the section along 120.75° E (*red solid line*), with **a** 0-, **b** 1-, and **c** 2-month lag, respectively. Areas with insignificant correlation (correlation coefficient > −0.3) were masked

when the westward ULST increased and vice versa. However, the correlation decreased rapidly with the distance from the axis of the SCSWBC, and consequently, the correlation between the band-passed ULST and section-integrated SCSWBC transport was only 0.18 with a 1- to 2-month lag (Fig. 15). Significant values less than −0.3 (above 95 % confidence level) mostly concentrated in the northern and western slopes of the SCS, with an extension around the southwest corner of the SCS deep basin. The ribbons of high negative values signify the direct impact of the ULST on the SCSWBC. However, in the El Niño winter of 1997, the westward ULST strengthened with a negative anomaly (the red line in Fig. 15), while a weakened winter monsoon over the SCS also occurred at the same time (the red line in Fig. 12c). As a net result, the southward SCSWBC transport decreased (the blue line in Fig. 15) responding primarily to the anomalous monsoon wind rather than the ULST. Similar cases also happened in the winter of 2004 as well as the summer of 2002 and 2009. It implied that the role of the ULST in modulating the interannual variability of the SCSWBC could be secondary in comparison with the wind over the SCS. This is consistent with the finding of Xu and Oey (2015) for seasonal variability.

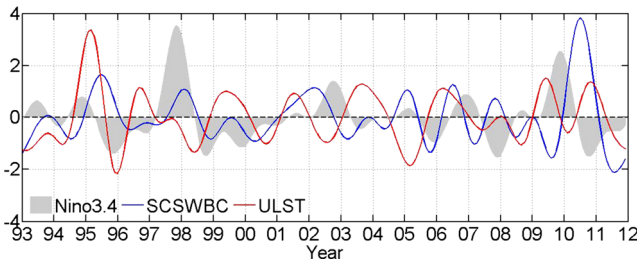

Fig. 15 Band-passed SCSWBC transport (*blue*), ULST (*red*), and Nino3.4 index (*shaded*). All time series were normalized by subtracting their mean value and then being divided by their standard deviation

5 Summary

In this paper, we attempted to differentiate the currents in the western SCS based on their dynamic origins and thereby designated only the current on the slope as the SCSWBC but regarded the flows on the western Sunda Shelf, which responded directly to the local wind stress, as part of the shelf circulation. The main features and variability of the SCSWBC from 1992 to 2011 were studied by using the REDOS data and observations. Controlled by the prevailing monsoonal winds and in- and outflows, the SCSWBC in winter flowed along the continental slope in the north and west, which reached its maximum intensity on the slope southeast of Vietnam, while in summer, the southward SCSWBC merged with the northward coastal current to form the VOC at about 12° N, which cut off a southern extension of the WBC on the slope. At 13.8° N off the central Vietnam coast, the SCSWBC was generally wider but shallower, and the core of the current was slightly closer to shore in the winter than in the summer.

Moreover, the structure of this current, including the axis, the width, and the maximum depth, varied significantly from year to year. In most of the El Niño winters, the SCSWBC tended to deepen and became narrower than that in the following winters. For most of the El Niño decaying summers, the SCSWBC deepened more markedly and got wider than that in the developing summers. The strength of the SCSWBC also showed a pronounced interannual difference, especially for the years when El Niño occurred. Based on a regression equation between the transport and the SLD, the SCSWBC transport off the coast of Vietnam was estimated to be −11.8 ± 3.5 Sv in winter and −3.0 ± 1.6 Sv in summer. The transport decreased by about 20 % in the El Niño developing winter and increased by about 18 % in the following winter. As to the decaying phase summers of 1995, 1998, and 2010, the SCSWBC retracted with the inner slope dominated by northward flows. The interannual variability of the monsoonal

forcing over the SCS, which was closely associated with the El Niño events, was proven to modulate the interannual variability of the SCSWBC transport significantly, whereas the impact of the remote ULST forcing was secondary.

Although the influencing factors and their relative importance in regulating the interannual variability of the SCSWBC were explored in the present work, the detailed dynamic mechanisms are still not fully understood and warrant further studies in the future. For example, the energy transfer between the basin-wide wind field and SCSWBC and the role of Rossby waves and eddies should be examined. Moreover, the Kuroshio intrusion affects the SCSWBC not only in the sense of the LST but also as eddies. How eddy activities vary and how they modulate the variability of the WBC still need to be investigated.

Acknowledgments The study is supported by projects 41476013 from the National Natural Science Foundation of China and XDA10010304 from the Strategic Priority Research Program of the Chinese Academy of Sciences. The authors would like to thank the AVISO, PSMSL, UHSLC, and CCMP groups for providing their data publicly.

References

Andres M, Park JH, Wimbush M, Zhu X, Chang KI, Ichikawa H (2008) Study of the Kuroshio/Ryukyu current system based on satellite-altimeter and in situ measurements. J Oceanogr 64:937–950

Atlas R, Hoffman RN, Ardizzone J, Leidner SM, Jusem JC, Smith DK, Gombos D (2011) A cross-calibrated, multiplatform ocean surface wind velocity product for meteorological and oceanographic applications. Bull Am Meteorol Soc 92:157–174

Cai S, Su J, Long X, Wang S, Huang Q (2005) Numerical study on the summer circulation of the upper South China Sea and its establishment. Acta Oceanol Sin 24:31–38

Cai S, Long X, Wang S (2007) A model study of the summer southeast Vietnam offshore current in the southern South China Sea. Cont Shelf Res 27:2357–2372

Carton JA, Chepurin G, Cao X, Giese BS (2000a) A simple ocean data assimilation analysis of the global upper ocean 1950–95. Part I: methodology. J Phys Oceanogr 30:294–309

Carton JA, Chepurin G, Cao X (2000b) A simple ocean data assimilation analysis of the global upper ocean 1950–95. Part II: results. J Phys Oceanogr 30:311–326

Chang YL, Oey LY (2011) Interannual and seasonal variations of Kuroshio transport east of Taiwan inferred from 29 years of tide-gauge data. Geophys Res Lett 38:L08603. doi:10.1029/2011GL047062

Chang CWJ, Hsu H, Wu C, Sheu W (2008) Interannual mode of sea level in the South China Sea and the roles of El Nino and El Nino Modoki. Geophys Res Lett 35:L03601. doi:10.1029/2007GL032562

Chen C, Wang G (2014) Interannual variability of the eastward current in the western South China Sea associated with the summer Asian monsoon. J Geophys Res 119:5745–5754

Chen G, Xue H (2014) Westward intensification in marginal seas. Ocean Dyn 64:337–345

Chu PC, Li R (2000) South China Sea isopycnal-surface circulation. J Phys Oceanogr 30:2419–2438

Chu PC, Chen Y, Lu S (1998) Wind-driven South China Sea deep basin warm-core/cool-core eddies. J Oceanogr 54:347–360

Chu PC, Edmons NL, Fan C (1999) Dynamical mechanisms for the South China Sea seasonal circulation and thermohaline variabilities. J Phys Oceanogr 29:2971–2991

Chu X, Xue H, Qi Y, Chen G, Mao Q, Wang D, Chai F (2014) An exceptional anticyclonic eddy in the South China Sea in 2010. J Geophys Res 119:881–897

Crosby DS, Breaker LC, Gemmill WH (1993) A proposed definition for vector correlation in geophysics: theory and application. J Atmos Ocean Technol 10:355–367

Dale WL (1956) Wind and drift currents in the South China Sea. Malays J Trop Geogr 8:1–31

Ducet N, Traon PYL, Reverdin G (2000) Global high-resolution mapping of ocean circulation from TOPEX/Poseidon and ERS-1 and -2. J Geophys Res 105:19477–19498

Fang G, Fang W, Fang Y, Wang K (1998) A survey of studies on the South China Sea upper ocean circulation. Acta Oceanogr Taiwan 37:1–16

Fang W, Fang G, Shi P, Huang Q, Xie Q (2002) Seasonal structures of upper layer circulation in the southern South China Sea from in situ observations. J Geophys Res 107:3202. doi:10.1029/2002JC001343

Fang W, Guo J, Shi P, Mao Q (2006) Low frequency variability of South China Sea surface circulation from 11 years of satellite altimeter data. Geophys Res Lett 33:L22612. doi:10.1029/2006GL027431

Fang G, Wang Y, Wei Z, Fang Y, Qiao F, Hu X (2009) Interocean circulation and heat and freshwater budgets of the South China Sea based on a numerical model. Dyn Atmos Oceans 47:55–72

Fang G, Wang G, Fang Y, Fang W (2012) A review on the South China Sea western boundary current. Acta Oceanol Sin 31:1–10

Gan J, Qu T (2008) Coastal jet separation and associated flow variability in the southwest South China Sea. Deep Sea Res, Part I 55:1–19

Gan J, Li H, Curchister EN, Haidvogel DB (2006) Modeling South China Sea circulation: response to seasonal forcing regimes. J Geophys Res 111:C06034. doi:10.1029/2005JC003298

Guo Z, Yang T, Qiu D (1985) The South China Sea warm current and the SW-ward current on its right side in winter. Trop Oceanol 4:1–9 **(in Chinese with English abstract)**

He Z, Wang D (2007) Surface pattern of the South China Sea western boundary current in winter. Adv Geosci 12:99–107

Holgate SJ, Matthews A, Woodworth PL, Rickards LJ, Tamisiea ME, Bradshaw E, Foden PR, Gordon KM, Jevrejeva S, Pugh J (2013) New data systems and products at the permanent service for mean sea level. J Coast Res 29:493–504

Huang Q, Wang W, Fu S, Chen R, Li Y, Zhou G (1997) A westward current that flows through the north of the Dongsha Islands in summer. Trop Oceanol 16:58–66 **(in Chinese with English abstract)**

Imawaki S, Uchida H, Ichikawa H, Fukasawa M, Umatani S, ASUKA Group (2001) Satellite altimeter monitoring the Kuroshio transport south of Japan. Geophys Res Lett 28:17–20

Large WG, McWilliams JC, Doney SC (1994) Oceanic vertical mixing: a review and a model with a nonlocal boundary layer parameterization. Rev Geophys 32:363–403

Li L, Wu R, Guo X (2000) Seasonal circulation in the South China Sea—a TOPEX/POSEIDON satellite altimetry study. Acta Oceanol Sin 22:13–26 **(in Chinese with English abstract)**

Li Y, Han W, Wilkin JL, Zhang W, Arango H, Zavala-Garay J, Levin J, Castruccio FS (2014) Interannual variability of the surface summertime eastward jet in the South China Sea. J Geophys Res 119:7205–7228

Liu Q, Yang H, Liu Z (2001a) Seasonal features of the Sverdrup circulation in the South China Sea. Prog Nat Sci 11:202–206

Liu Z, Yang H, Liu Q (2001b) Regional dynamics of seasonal variability in the South China Sea. J Phys Oceanogr 31:272–284

Masumoto Y, Sasaki H, Kagimoto T, Komori N, Ishida A, Sasai Y, Miyama T, Motoi T, Mitsudera H, Takahashi K, Sakuma H, Yamagata T (2004) A fifty-year eddy-resolving simulation of the

world ocean—preliminary outcomes of OFES (OGCM for the earth simulator). J Earth Simul 1:35–56

Qiu D, Yang T, Guo Z (1984) A west-flowing current in the northern part of the South China Sea in summer. Trop Oceanol 3:65–73 **(in Chinese with English abstract)**

Qu T (2000) Upper-layer circulation in the South China Sea. J Phys Oceanogr 30:1450–1460

Qu T, Mitsudera H, Yamagata T (2000) Intrusion of the North Pacific waters into the South China Sea. J Geophys Res 105:6415–6424

Qu T, Kim YY, Yaremchuk M, Tozuka T, Ishida A, Yamagata T (2004) Can Luzon Strait transport play a role in conveying the impact of ENSO to the South China Sea? J Clim 17:3643–3656

Qu T, Song YT, Yamagata T (2009) An introduction to the South China Sea throughflow: its dynamics, variability, and application for climate. Dyn Atmos Oceans 47:3–14

Shaw P, Chao S (1994) Surface circulation in the South China Sea. Deep-Sea Res 41:1663–1683

Shaw P, Chao S, Fu L (1999) Sea surface height variations in the South China Sea from satellite altimetry. Oceanol Acta 22:1–17

Shu Y, Xue H, Wang D, Chai F, Xie Q, Yao J, Xiao J (2014) Meridional overturning circulation in the South China Sea envisioned from the high-resolution global reanalysis data GLBa0.08. J Geophys Res 119:3012–3028

Shu Y, Xue H, Wang D, Xie Q, Chen J, Li J, Chen R, He Y, Li D (2016) Observed evidence of the anomalous South China Sea western boundary current during the summer of 2010 and 2011. J Geophys Res 121:1145–11

Stommel H (1948) The westward intensification of wind-driven ocean currents. Trans Am Geophys Union 29:202–206

Su J (2004) Overview of the South China Sea circulation and its influence on the coastal physical oceanography outside the Pearl River Estuary. Cont Shelf Res 24:1745–1760

Sverdrup HU (1947) Wind-driven currents in a baroclinic ocean: with application to the equatorial currents of the eastern Pacific. Proc Natl Acad Sci U S A 33:318–326

Tian J, Yang Q, Liang X, Xie L, Hu D, Wang F, Qu T (2006) Observation of Luzon Strait transport. Geophys Res Lett 33:L19607. doi:10.1029/2006GL026272

Wang B, Wu R, Fu X (2000) Pacific–East Asian teleconnection: how does ENSO affect East Asian climate? J Clim 13:1517–1536

Wang G, Chen D, Su J (2006a) Generation and life cycle of the dipole in the South China Sea summer circulation. J Geophys Res 111: C06002. doi:10.1029/2005JC003314

Wang Y, Fang G, Wei Z, Qiao F, Chen H (2006b) Interannual variation of the South China Sea circulation and its relation to El Niño, as seen from a variable grid global ocean model. J Geophys Res 111: C11S14. doi:10.1029/2005JC003269

Wang G, Xie S, Qu T, Huang R (2011) Deep South China Sea circulation. Geophys Res Lett 38:L05601. doi:10.1029/2010GL046626

Wang H, Wang D, Liu G, Wu H, Li M (2012) Seasonal variation of eddy kinetic energy in the South China Sea. Acta Oceanol Sin 31:1–15

Wang D, Liu Q, Xie Q, He Z, Zhuang W, Shu Y, Xiao X, Hong B, Wu X, Sui D (2013) Progress of regional oceanography study associated with western boundary current in the South China Sea. Chin Sci Bull 58:1205–1215

Wu C, Chang CWJ (2005) Interannual variability of the South China Sea in a data assimilation model. Geophys Res Lett 32:L17611. doi:10.1029/2005GL023798

Wu C, Shaw P, Chao S (1998) Seasonal and interannual variations in the velocity field of the South China Sea. J Oceanogr 54:361–372

Wyrtki K (1961) Physical oceanography of the Southeast Asian waters. NAGA Report 2. San Diego: eScholarship Repository, Scripps Institute of Oceanography, University of California

Xie S, Xie Q, Wang D, Liu WT (2003) Summer upwelling in the South China Sea and its role in regional climate variations. J Geophys Res 108:3261. doi:10.1029/2003JC001867

Xing Y, Cheng G, Shu Y, Wang D (2012) Anomalous characteristics of the ocean circulation in South China Sea during the El Niño events. Oceanol Limnol Sin 43:201–210 **(in Chinese with English abstract)**

Xu F, Oey LY (2015) Seasonal SSH variability of the northern South China Sea. J Phys Oceanogr 45:1595–1609

Xu X, Zhang Q, Chen H (1982) The general descriptions of the horizontal circulation in the South China Sea. In: Proceeding of the 1980 Symposium on Hydrology and Meteorology of the Chinese Society for Oceanology and Limnology. Beijing: Science Press, 137–145 **(in Chinese with English abstract)**

Xue H, Chai F, Pettigrew N, Xu D, Shi M, Xu J (2004) Kuroshio intrusion and the circulation in the South China Sea. J Geophys Res 109: C02017. doi:10.1029/2002JC001724

Yang H, Liu Q, Liu Z, Wang D, Liu X (2002) A general circulation model study of the dynamics of the upper ocean circulation of the South China Sea. J Geophys Res 107:3085. doi:10.1029/2001JC001084

Yang Q, Tian J, Zhao W (2010) Observation of Luzon Strait transport in summer 2007. Deep Sea Res, Part I 57:670–676

Yaremchuk M, Qu T (2004) Seasonal variability of the large-scale currents near the coast of the Philippines. J Phys Oceanogr 34:844–855

Yuan Y, Liao G, Yang C (2008) The Kuroshio near the Luzon Strait and circulation in the northern South China Sea during August and September 1994. J Oceanogr 64:777–788

Zeng X, Peng S, Li Z, Qi Y, Chen R (2014) A reanalysis dataset of the South China Sea. Sci Data 1:140052. doi:10.1038/sdata.2014.52

Zhang Z, Zhao W, Tian J, Yang Q, Qu T (2015) Spatial structure and temporal variability of the zonal flow in the Luzon Strait. J Geophys Res 120:759–776

Zhou H, Yuan D, Li R, He L (2010) The western South China Sea currents from measurements by Argo profiling floats during October to December 2007. Chin J Oceanol Limnol 28:398–406

Zhu X, Ichikawa H, Ichikawa K, Takeuchi K (2004) Volume transport variability southeast of Okinawa Island estimated from satellite altimeter data. J Oceanogr 60:953–962

Zhu X, Zhao R, Guo X, Long Y, Ma Y, Fan X (2015) A long-term volume transport time series estimated by combining in situ observation and satellite altimeter data in the northern South China Sea. J Oceanogr 71:663–673